

Article

Theoretical Discourse on Producing High Temporal Yields of Nuclear Excitations in Cosmogenic ^{26}Al with a PW Laser System: The Pathway to an Astrophysical Earthbound Laboratory

Klaus Michael Spohr ^{1,*}, Domenico Doria ¹  and Bradley Stewart Meyer ²

¹ Extreme Light Infrastructure (ELI-NP) & Horia Hulubei National Institute for R & D in Physics and Nuclear Engineering (IFIN-HH), Str. Reactorului No. 30, P.O. Box MG-6, 077125 Bucharest– Măgurele, Romania; domenico.doria@eli-np.ro

² Department of Physics and Astronomy, Clemson University, Clemson, SC 29634-0978, USA; mbradle@clemson.edu

* Correspondence: klaus.spohr@eli-np.ro; Tel.: +40-21-404-2301

Received: 7 November 2018; Accepted: 14 December 2018; Published: 26 December 2018



Abstract: The development of the 10 PW laser system at the Extreme Light Infrastructure is a crucial step towards the realization of an astrophysical Earthbound laboratory. The interaction of high-power laser pulses with matter results in ultrashort (fs-ps) pulses of 10s of MeV ions and radiation that can create plasma and induce nuclear reactions therein. Due to the high fluxes of reaction-driving beam pulses, high yields of radioactive target nuclei in their ground and excited states can be provided in situ on short time scales. Cosmogenic ^{26}Al , which is of pronounced astrophysical interest, is a prime candidate for evaluating these new experimental possibilities. We describe how, for a short duration of $\Delta t \sim 200$ ps, laser-driven protons with energies above $E_p \sim 5$ MeV can induce the compound nucleus reaction $^{26}\text{Mg}(p, n)^{26}\text{Al}$ leading to high and comparable yields of the three lowest-lying states in ^{26}Al including the short-lived, $t_{1/2} = 1.20$ ns state at 417 keV. In the aftermath of the reaction, for a short duration of $t \sim$ ns, the yield ratios between the ground and the two lowest-lying excited states will resemble those present at thermodynamic equilibrium at high temperatures, thus mimicking high ^{26}Al entropies in cold environments. This can be seen as a possible first step towards an investigation of the interplay between those states in plasma environments. Theory suggests an intricate coupling of the ground state $^{26}\text{Al}_{g.s.}$ and the first excited isomer ^{26m}Al via higher-lying excitations such as the $J = 3^+$ state at 417 keV resulting in a dramatic reduction of the effective lifetime of ^{26}Al which will influence the isotope's abundance in our Galaxy.

Keywords: laser-induced nuclear reactions; high-power laser systems; laser plasma; nuclear astrophysics; effective lifetime; ^{26}Al

1. Introduction

Laboratory measurements of nuclear reaction rates are made on target nuclei in their ground states. However, in stellar plasma conditions which govern the evolution of abundances in the Universe, the reacting nuclei are distributed among their excited states. Without providing these conditions, a proper experimental accounting of stellar models remains elusive. Nonetheless, direct experiments on the interplay of ground and excited states relevant for nuclear astrophysics have so far escaped scientific investigation since such studies are extremely difficult to realize in Earthbound laboratories driven by existing RF-based accelerator systems. This is mainly due to the short-lived, fs–ns nature of the relevant excited nuclear states in conjunction with the overall rather low instantaneous beam

intensities deliverable by RF-based accelerator systems during that short timescales which result in low spontaneous yields for the promptly decaying excited states. As of today, reaction rate evaluations on excited states have not been measured and theory relies therefore on Hauser-Feshbach calculations [1] in which an assumption of a thermal population of excited states is undertaken. This approach is deemed to be very crude in general and is certainly incorrect for a handful of isotopes that have longer-lived isomers and for which internal thermalization does not therefore easily occur. For such nuclei, the equilibration of the longer-lived isomer and the ground state (g.s.) occurs only indirectly via upper-lying levels at high temperatures in the MK to GK regime. The cosmogenic ^{26}Al , the subject of this investigation, is perhaps the most prominent case in nuclear astrophysics for this kind of nuclei.

In the following discourse, we depict how the new generation of all-optical, high-power laser systems (HPLSs) based on chirped pulse amplification (CPA) invented by Strickland and Mourou [2] can address the problem of providing short-lived states with considerably high yields and hence can promote astrophysical research in the future.

2. Production and Decay of Cosmogenic ^{26}Al

2.1. Spontaneous Yields

Core to the depicted concept is the high spontaneous flux of ion-driven reactions as provided by a single short pulse from a HPLS which leads to high temporal yields $Y_i^d(t)$ of excited states by direct population (d) in a nucleus. Assuming that all nuclear levels are numbered subsequently according to their energy E_i , we find for the direct population of the i -th state;

$$Y_i^d(t) = N \cdot \sigma_i \cdot \phi \cdot (1/\lambda_i) \cdot \begin{cases} (1 - \exp(-\lambda_i \cdot t)), & \text{for } t < t_{\text{irrad}}, \\ [1 - \exp(-\lambda_i \cdot t_{\text{irrad}})] \cdot \exp(-\lambda_i \cdot (t - t_{\text{irrad}})), & \text{for } t \geq t_{\text{irrad}}; \end{cases} \quad (1)$$

wherein N is the number of atoms exposed to the beam in the irradiated sample, σ_i the energy dependent cross-section for the direct population of the i -th state in barns, ϕ the beam flux and λ_i the total decay rate of the i -th level in s^{-1} . The parameter t_{irrad} represents the irradiation time during which the beam of incoming particles triggers the reaction. For simplification, all the aforementioned parameters are seen to be time-independent and thus constant during t_{irrad} . The factor $(t - t_{\text{irrad}})$ is the time elapsed after the production of a specific nucleus and its states via an irradiating beam has stopped. Equation (1) is valid as long as $\sigma_i \cdot \phi \ll \lambda_i$ which is the case even for the high, instantaneous beam fluxes, ϕ that are achievable with a HPLS. Equation (1) only describes the direct population of the i -th state by the reaction-driving pulse and needs to be extended if an indirect population (feeding) of this state via higher-lying energetic states occurs. For this more general case, the total yield $Y_i(t)$ for the i -th state, assuming that $1 \leq i < k \leq N_{\text{tot}}$, can be calculated via,

$$Y_i(t) = Y_i^d(t) + \sum_{k>i}^{N_{\text{tot}}} f_{ki} \cdot \int_0^t |A_k(t')| dt' \quad (2)$$

in which

$$A_k(t') = -\frac{dY_k(t')}{dt'} \quad (3)$$

is the instantaneous activity of the feeding state k with half-life λ_k and f_{ki} the partial branching ratio of the k -th state to the i -th state. The variable N_{tot} describes the total number of states in the nucleus which feed into the level at E_i . For complex systems in which a long decay chain with constant initial activities $A_k(0)$ exists, Equation (2) will result in the Bateman equation for the i -th state [3]. To include the possibility that the feeding state at E_k is also directly populated by the flux of particles with a specific

cross-section of σ_k , the instantaneous activity $A_k(t')$ defined in Equation (3) was used in Equation (2) for the calculations in this work. We also exclude the possibility of any induced upward transitions from E_i to the higher-lying states at E_k via photo-absorption as no extremely hot equilibrated plasma condition can be provided by a HPLS for which those photo-absorption processes would appear with high enough yields to change Y_i .

Equation (1) shows Y_i scales linear with ϕ . Experiments show that $\sim 10^{8-9}$ times higher values for the spontaneous beam fluxes ϕ are achievable with HPLS if compared to typical values associated RF-based technology. Though these extremely high fluxes can only be delivered for ultrashort irradiation time spans t_{irrad} which are in the order of the lifetime of short-lived states, the resulting enhancement in the presented case, $t_{1/2} = 1.20$ ns level at 417 keV in ^{26}Al , will still be in the order of 10^{7-8} larger when compared to a DC or RC beam from a conventional accelerator system, since the crucial factor $[1 - \exp(-\lambda \cdot t_{\text{irrad}})]$ is still around ~ 0.1 . The other important factor in Equation (1) is the exponential decline after t_{irrad} which is given by the term $\exp(-\lambda \cdot (t - t_{\text{irrad}}))$. This term expresses the fact that any time-resolved probing of the interplay of states including short-lived isomers must occur within a short timeframe itself, which can only be realized by a generically short probing pulse as provided by a HPLS. Therefore, to allow such kinds of studies at e.g., the Extreme Light Infrastructure for Nuclear Physics (ELI-NP), two synchronized laser beamlines are implemented. The possibility of ultrafast probing is another unique feature of HPLS-technology.

In addition to a direct reaction-induced production of a nuclear state, a population enhancement of states of interest can often be achieved via the feeding from states at higher energies as shown in Equation (2). This circumstance, which will become especially interesting once mono-energetic beams, can be delivered by a HPLS.

It is also important to note that Equation (1) only applies for a single pulse of short duration and the overall total reaction yields driven by a HPLS are some orders of magnitude smaller than those achievable with most of the RF-based systems over a prolonged experimental campaign. However, in summary, it is clear that if t_{irrad} is in the order of the lifetimes of short-lived excited states ($\tau_{\text{short}} = 1/\lambda_{\text{short}}$), their yields, relative to longer living, e.g., few seconds, or even stable states, can be optimized for time spans in the order of τ_{short} .

2.2. Yield Distributions of Excited States and Temperature Equivalents

The yield ratios between the ground and excited states can be mapped to a corresponding Maxwell-Boltzmann distribution describing a thermal equilibrium represented by a single temperature T via,

$$\frac{Y_2(t)}{Y_1(t)} = \frac{(2 \cdot J_2 + 1)}{(2 \cdot J_1 + 1)} \cdot \exp\left(-\frac{E_2 - E_1}{k_B T}\right), \quad (4)$$

in which Y_1 and Y_2 describe the state populations at a given time, J_1 and J_2 are the spin values of the nuclear states at the energies E_1 and E_2 . Equation (4) has been used for the matching of state populations to temperature values of evaporation fragments emitted from a compound nucleus after a fusion reaction. Thus, the appliance of this concept to laser-induced nuclear compound reactions seems more than adequate, especially as the time spans involved are similar to the typical interaction times which can be provided by a HPLS. The formation stage for the compound nucleus takes a period of time approximately equal to the time interval for the bombarding particle to travel across the diameter of the target nucleus which is $\sim 1 \times 10^{-21}$ s. After a relatively long period during which the compound system has thermally equilibrated which can extend up to 1×10^{-15} s, it disintegrates, usually into an ejected small particle and a larger evaporation fragment nucleus which inherits the compound's temperature represented by the corresponding value of $k_B T$. Thus, after a correction for the energy given to the rotational motion of the residuals is applied, one can deduce on the internal temperature of a reaction residual from its measured population ratio. The validity of this approach was e.g., demonstrated by Morrissey et al. [4] who proved that the population ratio does represent the internal temperature of a residual nucleus for a wide range of internal excitation energies. Hence, $k_B T$ will

represent the temperature of a nucleus if equilibrated in hot plasma. Obviously, in an experiment no hot plasma conditions can be provided in the matter surrounding the compound nucleus sustaining an equilibrium in a secondary reaction target. Therefore, the high value for $k_B T$ within the nucleus will only prevail for the fleeting time spans associated with the shortest lifetimes of the decaying excited states that were populated. High-power laser accelerators can create this special state of synthetic entropy condition where we will find a gamut of hot nuclei in their short-lived excited states in a surrounding cold environment after a reaction-triggering laser pulse. During the associated short time spans the temperature, which was present in the nuclear matter at time of the evaporation, is normally equivalent to $k_B T$ values in the MeV regime which equates to hot plasma temperatures in the GK region. It is worth noting that of course one can produce excited states in nuclei, for example via nuclear reactions or beta decay, or in-flight whereby γ -rays are detected with arrays of germanium detectors around a target position with RF-based technology. However, it is the provision of high spontaneous yields which makes a HPLS an interesting tool for selected cases of nuclei in which the equilibrium studies on thermalized conditions are particularly hard to achieve due to the interplay of long- and short-lived isomers. Moreover, the high temporary yields of hot evaporation residues can, in principle, be probed by a secondary ion- or γ -beam originating from a second synchronized laser pulse. We again must stress the fact that no real plasma environment at hot temperatures will exist in such a hypothetical experiment; it is just the population distributions of the excited states in plasma which is mimicked by the inheritance of the compound nucleus' temperature.

The cosmogenic ^{26}Al , was chosen for this evaluation due to its importance for astrophysics and some already existing or soon to be published experimental work [5,6]. Our work here will give an answer to the long-standing questions: "What is a unique feature of all-optical PW accelerators which cannot be achieved with traditional RF-based accelerator technology and how can the CPA technology invented by Strickland and Mourou be best applied to enrich fundamental nuclear physics research?". We believe that we can answer this question satisfactorily as we depict the unique ability of high-intensity laser acceleration to allow the production of high temporal yields of ultrashort-lived nuclear species in their ground and excited states, which is a crucial step towards the realization of an astrophysical laboratory. The supply of high yields of short-lived states positively distinguishes HPLS-driven accelerators from standard RF-based technology. In the future, these states can be may subjected to further probing by e.g., creating a low-temperature plasma environment such as WDM during the reaction processes or using an ultraintense probing X-ray beam in coincidence. Moreover, our work will show that already existing TW and PW laser-driven systems can be used to measure hitherto elusive in situ nuclear reaction rates in plasma to underpin astrophysical theory. As such, the presented discourse promotes future nuclear research at facilities such as ELI-NP and elucidates how they will help understanding of the complex chemical evolution within our Galaxy. In this respect one needs to point out that it is e.g., already possible to create warm dense-matter conditions in the laboratory [7,8]. Even the study of exotic fusion-fission reactions in the quest to produce very neutron-rich isotopes to understand the production of heavy nuclei in the Universe [9] is envisaged at ELI-NP.

2.3. The Importance of ^{26}Al for Astrophysics

To understand the astrophysical abundances in our Galaxy, the cosmogenic isotope ^{26}Al is of outstanding astrophysical significance as it is a core isotope for γ -ray astronomy [10]. Its presence in the Galaxy was discovered by Mahoney et al. [11]. Theoretically, the isotope derives from explosive helium, carbon, oxygen, and silicon burning cycles [12], as well as novae or supernovae explosions, Wolf-Rayet Stars, red giants, and supermassive stars [13,14]. Moreover, the correlated excesses of its daughter product ^{26}Mg in comparison with stable ^{27}Al provide important constraints on the formation time of primitive meteorites and components therein [15–17]. The total galactic abundance of ^{26}Al is estimated to be around $2 M_\odot$ to $3 M_\odot$. State-of-the-art theories only account for a fraction of this value. A study of the effective lifetime τ_{eff} of ^{26}Al is henceforth necessary. Any related experimental

investigation must account for the rather unique and complex decay pattern of the isotope which is sketched in Figure 1.

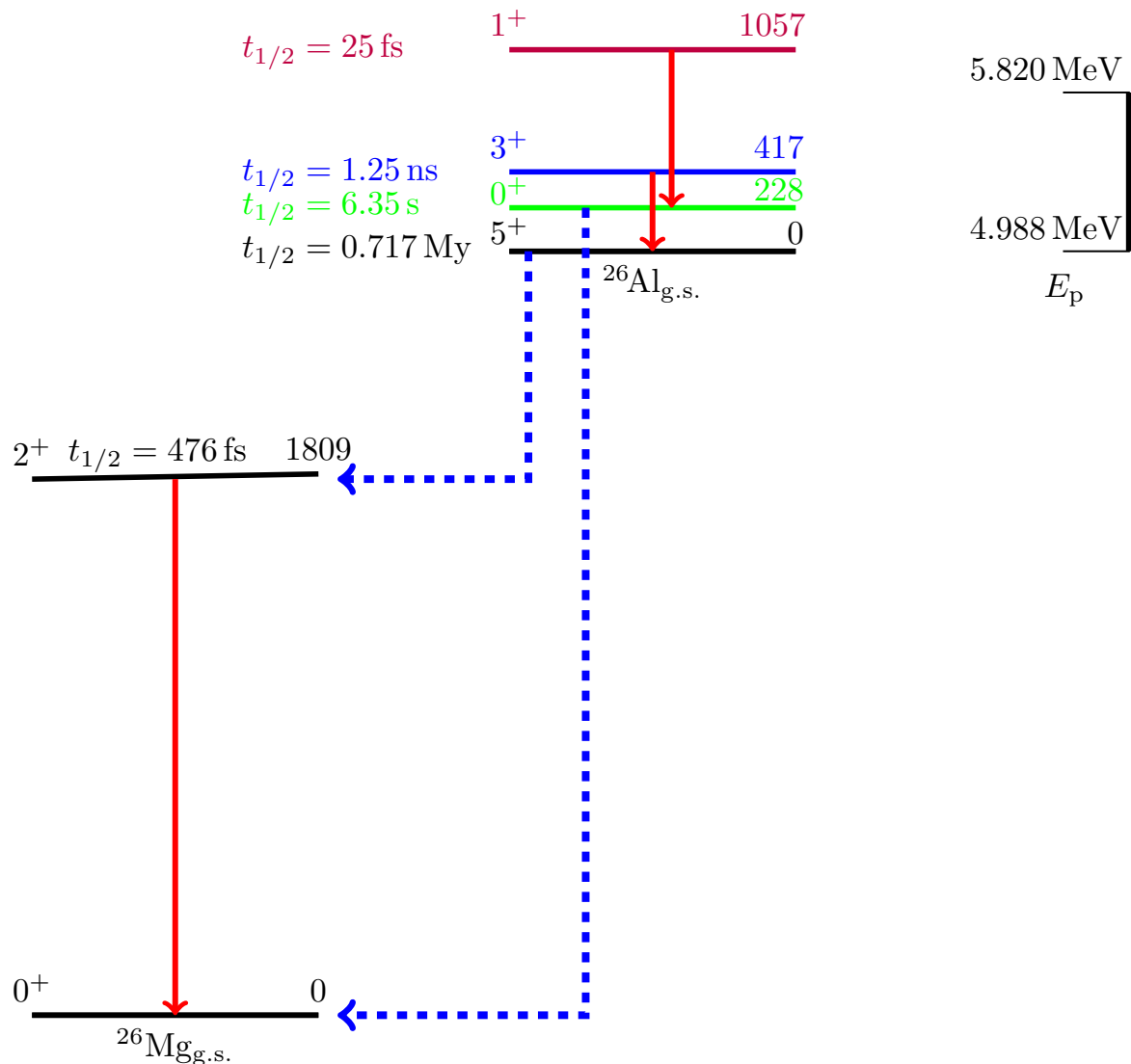


Figure 1. Simplified decay pattern of ^{26}Al including the lowest four states. The two β^+ decay branches are depicted with the blue dotted lines. The γ -transitions between the states are indicated with red arrows, such as the 417 keV state which solely decays into the ground state $^{26}\text{Al}_{\text{g.s.}}$. To the right of the level scheme, the proton energy range $4.988 \text{ MeV} \leq E_p \leq 5.820 \text{ MeV}$ surveyed for the reaction $^{26}\text{Mg}(p,n)^{26}\text{Al}$ by Skelton et al. is depicted [18].

In cold environments, ^{26}Al decays via two prominent β^+ decay routes from its ground and first excited state which are characterized by very different values of their degree of forbiddenness. This special scenario complicates the evaluation of the effective ^{26}Al decay rate λ_{eff} in a stellar plasma as one cannot assume the first two states existed in an equilibrated thermal distribution. Specifically, the decay from its $J = 5^+$ ground state is a second-order forbidden β^+ decay with a corresponding long half-life of $t_{1/2} = 0.717$ My leading to a branching of 97.24% to the first excited state in ^{26}Mg at 1809 keV. The β^+ decay is followed by a quasi-prompt emission ($t_{1/2} = 476$ fs) of the corresponding γ -ray in ^{26}Mg . It was this transition which was discovered by Mahoney et al. with the HEAO-3 satellite surveying the radiation background of the Galaxy in 1984 [11]. On the other hand, the first excited state of ^{26}Al at 228 keV ($^{26\text{m}}\text{Al}$) decays via a rather fast ($t_{1/2} (^{26\text{m}}\text{Al}) = 6.35$ s) super-allowed $0^+ \rightarrow 0^+$ β^+ decay directly into the stable ground state $^{26}\text{Mg}_{\text{g.s.}}$. Due to the high spin difference,

a direct electromagnetic transition from the 228 keV level to the ground state $0^+ \rightarrow 5^+$ in ^{26}Al has an extremely low transition probability and, as such, one is forced to treat the decay of $^{26}\text{Al}_{\text{g.s.}}$ and $^{26\text{m}}\text{Al}$ as different species in theoretical evaluations. To shed light on the overall destruction of ^{26}Al one needs to estimate the interplay between these two states in hot environments to be able to calculate the effective decay rate λ_{eff} in stellar plasma.

Theory predicts that a thermal equilibrium between the long-lived 5^+ ground state and the first isomeric 0^+ state at 228 keV will occur at high temperatures (1×10^6 K to 1×10^9 K) via a manifold of interlinking high-energy transitions which induce a population of short-lived (fs–ns) high-lying energy levels. This will result in a much shorter τ_{eff} for the ^{26}Al in hot environments. The groundwork of this interpretation was done by Ward and Fowler [19], followed by a more complex analysis by Coc et al. in 1999 [20]. Both efforts are cited in the most elaborated work to date, which focuses on the decay of ^{26}Al in thermodynamic equilibrium by Gupta and Meyer [21]. In that work a new, holistic approach that introduces a dissection of the structure of ^{26}Al into two different ensembles e_1 and e_2 is based on whether the most prominent decay path feeds into the ground state (e_1) or the first excited state (e_2) at cold temperatures. They then calculate in detail how these two ensembles start to merge into a single Maxwell-Boltzmann distribution. In detail, the authors evaluated the Einstein coefficients of induced absorption between the lowest-lying 64 states in ^{26}Al which allows the determination of the effective transition rate between the two assumed species represented by e_1 and e_2 , labelled λ_{12} for ^{26}Al as a function of temperature T . Their results show that below $T \sim 0.4$ GK the $^{26\text{m}}\text{Al}$ metastable state has no chance to equilibrate with the ground state before decaying via $^{26\text{m}}\text{Al}$. The scenario dramatically changes above $T \sim 0.4$ GK where internal equilibration of ^{26}Al competes with the β^+ decay from the metastable $^{26\text{m}}\text{Al}$ thus influencing the transition between the two species. This equilibration leads to a much-enhanced λ_{eff} . The increase of λ_{eff} between 0.1 GK to 10 GK is around 25 orders of magnitude ($1 \times 10^{-10} \text{ s}^{-1}$ to $1 \times 10^{15} \text{ s}^{-1}$) thus underpinning the need to find experimental pathways for investigations. It is, however, clear that a technical realization of such a hot plasma in the above-cited temperature regime will experimentally remain elusive for the foreseeable future. However, the production of the short-lived states via the decay of a hot nuclear compound results in the production of sufficiently high yields of the excited 417 keV 3^+ state, comparable to those of the first two states in ^{26}Al for a duration of several ns (see Equation (1)). According to Gupta and Meyer, the aforementioned 2^{nd} excited state plays the most crucial role in steering the equilibration between the two ensembles. As such, the provision of the short-lived 417 keV isomer with high yield can be seen as a first step towards measurements at short-lived excited states and their interplay with longer-lived states. This scenario will become particularly interesting if, in future, high fluxes of fs-long probing X-rays can be delivered in coincidence with the production of the excited states or warm dense-matter conditions (WDM) with the driving proton beams. Again, in both cases, no extremely hot plasma conditions will exist but still such investigations must be seen as experimental stepping stones on the pathway to an astrophysical laboratory.

2.4. Cross-Section of ^{26}Al and its Production in Laser Plasma Experiments

The most effective way to produce ^{26}Al in situ is by harvesting laser-induced proton acceleration. In the associated compound nucleus reaction $^{26}\text{Mg}(p, n)^{26}\text{Al}$ in which the formed compound nucleus ^{27}Al is excited by the energy above the reaction threshold of the impacting proton. The emittance of a neutron in the exit channel leads to excited states in ^{26}Al as well as directly to the ground state $^{26}\text{Al}_{\text{g.s.}}$. Due to the prominence of this reaction, precise measurements of the individual cross sections for $^{26}\text{Al}_{\text{g.s.}}$, $^{26\text{m}}\text{Al}$ and the 3^+ level at 417 keV, $^{26}\text{Al}_{417}$, have been carried out over three decades ago by Skelton et al. [18]. Their experimental campaign facilitated an efficient neutron detector, the graphite-cube neutron-detection system (GCNDS) at the California Institute of Technology in Pasadena, CA, US. The cross-section measurements spanned over a proton energy range of almost 1 MeV from the reaction threshold at $E_p = 4.988$ MeV to $E_p = 5.820$ MeV (see Figure 1). A very precise average energy resolution for the cross sections of $\delta E = 2.5$ keV was achieved by measuring a total of

328 different energy values [22]. In detail they examined three different physical quantities to conclude on the reaction cross sections for the first three states in ^{26}Al . Details are displayed in Table 1. Therein n_{tot} refers to all neutrons emitted in the reaction process while n_{228} and n_{417} represent neutron channels that lead to the population of the first or second excited state at 228 keV and 417 keV respectively.

Based on the published data, the integral cross sections σ^{int} and their uncertainties for the three lowest-lying states in ^{26}Al were calculated in this work. The relative uncertainty, $\delta\sigma_{\text{g.s.}}^{\text{int}}/\sigma_{\text{g.s.}}^{\text{int}}$, of the integral cross-section for $^{26}\text{Al}_{\text{g.s.}}$, was found to be higher than those of the other two integral cross sections, as the integral cross section for the population of the ground state $\sigma_{\text{g.s.}}^{\text{int}}$ was not measured, but calculated from the difference of the measured total neutron yield and the sum of the yields for n_{417} and n_{228} . In the experiment it was not possible to directly measure the produced amount of $^{26}\text{Al}_{\text{g.s.}}$, an unfortunate restriction which will also apply for future high-power laser-based investigations. This is due to the overall low total production yield which will not allow a direct quantification of $\sigma_{\text{g.s.}}^{\text{int}}$. Firstly, the very long lifetime of $^{26}\text{Al}_{\text{g.s.}}$ does not permit the measurement of its decay with any radiation detector. Moreover, the expected total yields for the ground state will be in the order of $\sim 1 \times 10^5$ to $\sim 1 \times 10^7$ per pulse for a thick target which is still far below the sensitivity of conventional mass separators. The installation of an online isotope separation system including a Penning-trap; as e.g., depicted in [23] would allow to measure smallest amounts of $^{26}\text{Al}_{\text{g.s.}}$ that would emerge from a thin target after a laser pulse; could potentially address this issue. However, to our knowledge, such an online isotope separation system is not foreseen to be implemented at any upcoming HPLS worldwide in the near future.

Table 1. Calculated integral cross sections σ^{int} and methods used to measure $\sigma(E)$ for the lowest three states in ^{26}Al .

State	$\sigma^{\text{int}}/\text{MeVmb}$	Method Used in [18]
$\sigma_{\text{g.s.}}^{\text{int}}$	4.9(9)	Total neutron yield from the $^{26}\text{Mg}(p, n_{\text{tot}})^{26}\text{Al}$ reaction measured by the GCNDS. Note, due to the very long half-life of $^{26}\text{Al}_{\text{g.s.}}$, no delayed 511 keV annihilation radiation yield will be measurable emerging from the associated ground state decay.
$\sigma_{228}^{\text{int}}$	30.2(3)	Delayed 511 keV annihilation radiation yield from the $^{26}\text{Mg}(p, n_{228})^{26}\text{Al}$ reaction measured by two NaI(Tl) detectors in coincidence. An irradiation-count cycle with $t_{\text{irrad}} = 6$ s and $t_{\text{count}} = 30$ s was applied.
$\sigma_{417}^{\text{int}}$	19.3(9)	Prompt 417 keV γ -ray yield from the $^{26}\text{Mg}(p, n_{417})^{26}\text{Al}$ using an ultrathin target with a thickness of $8.5 \mu\text{gcm}^{-2}$. The prompt radiation was measured by a 60 cm^3 Ge(Li) detector.

We assume that integral cross sections will be valid for the high instantaneous fluxes ϕ of protons at a HPLS as plasma conditions will not prevail in the secondary target. The precise measurements as depicted by Skelton et al. [18] cannot be repeated at a HPLS for the foreseeable future. First and foremost, the systems are not capable of delivering high-flux pulses of reaction-driving mono-energetic protons with high frequency. Hence, overall yields and associated measurement statistics derived from a laser plasma experiment will lack behind the results obtainable with RF-based technology. Indeed, laser accelerators are best described as high-intensity low-repetition-rate systems if compared to RF-based technology. In addition, the most widely applied ion acceleration mechanism is the target normal sheath acceleration (TNSA) scheme as described by e.g., Wilks et al. [24]. Although proton energies of up to 100 MeV are achievable with TNSA [25], their proton energy distribution dN/dE_p inherits the Maxwell-Boltzmann energy distribution of the initially accelerated electrons and is therefore not mono-energetic, hence HPLS will practical allow only the measurement of integral cross sections at present.

Moreover, a direct efficient way of a measurement of neutrons in the way presented by Skelton et al. [18] is also not feasible for the time being at any existing PW laser site as they used a

highly efficient neutron detector surrounding the relatively small target chamber. For comparison, the target chambers used in high-power laser research will have a volume in the order of several m^3 and hence cannot be surrounded by a 4π detector system.

Additionally, during any proton pulse, an in situ measurement of the 417 keV transition is also not possible, as the initially produced proton beam coincides with intense soft and hard X-ray background radiation producing a strong electromagnetic pulse (EMP). Therefore, the only observable in a laser-driven ^{26}Al experiment will be the 511 keV delayed annihilation line, from which $\sigma_{228}^{\text{int}}$ can be derived. Nonetheless, we will be able to scale the presumed yields for the ground state and second excited state at 417 keV based on the calculated integral cross sections $\sigma_{\text{g.s.}}^{\text{int}}$ and $\sigma_{417}^{\text{int}}$ using the measured value of $\sigma_{228}^{\text{int}}$ as reference.

An inaugural *prima facie* experiment was undertaken with the Vulcan laser at the Rutherford Appleton Laboratory (RAL) in which the $^{26}\text{Mg}(p, n_{228})^{26\text{m}}\text{Al}$ reaction was studied with laser accelerated protons created by 300 TW pulses at a rate of $\sim f = 2 \times 10^{-4}$ Hz. Protons well above the reaction threshold at $E_p = 4.988$ MeV could be produced. A delayed γ -radiation line measured in situ at 511 keV with $t_{1/2}^{\text{exp}} = 6.6(3)$ s was unambiguously identified as the annihilation radiation associated with the β^+ decay of $^{26\text{m}}\text{Al}$. The total yield per pulse measured was as high as 5×10^5 of $^{26\text{m}}\text{Al}$. They produced nuclei were concentrated within a volume of ~ 0.08 cm^3 in the secondary MgO reaction target. For more details see [5,6].

3. Theoretical Evaluation of Achievable Population Distributions for the First Three Excited States in ^{26}Al in Laser Induced Plasma Experiments

3.1. General Considerations

Based on Equations (1) and (2) and the values of the integrated cross sections σ^{int} from Table 1, as well as the results of the inaugural experimental study, the achievable population yields of the lowest three states in ^{26}Al were theoretically estimated. A short proton irradiation period, $t_{\text{irrad}} = 200$ ps was assumed. To adjust such a short t_{irrad} in an experiment, one needs to place the ultrathin plastic sheets used as primary targets for proton production in very close proximity to the secondary reaction target, consisting of ^{26}Mg or ^{26}MgO in isotopically enriched form. This was applied in the aforementioned inaugural test experiment at RAL. In such close geometry one is able to minimize the spread in the time-of-flight, δt_{TOF} , between the most energetic protons produced and those that will be just above the reaction threshold at $E_p = 4.988$ MeV [6]. It is worth pointing out that the minimization of δt_{TOF} is crucial to provide a short t_{irrad} . Distances between the primary production target and the secondary reaction target of less than 1 cm are technically feasible to date. Choosing a much closer distance could mean that the secondary production target maybe damaged or even destroyed by a single laser pulse at high intensity. Obviously, the original 25 fs duration of the initial laser pulse which drives the proton production cannot be sustained, but with distances in the cm regime, δt_{TOF} values below 100 ps can be achieved. At any experiment one ideally would maximize the intensity of protons in the relevant energy rather than producing higher energetic protons with e.g., $E_p \geq 9$ MeV. Also, the high magnitude of protons with energies below the reaction threshold maybe facilitated in future experiments to create conditions of WDM in the volume within the secondary target where the reaction takes place. That alone is worth a consideration, as such scenarios cannot be achieved with conventional RF-based technology.

Isotopically enriched ^{26}Mg target comes at a high cost. Natural magnesium cannot be taken due to a series of intruder reaction channels which would make the identification of the $t_{1/2} = 6.35$ s decay of $^{26\text{m}}\text{Al}$ impossible. A crucial parameter is also the thickness of the ^{26}Mg target. To enhance the yield, one would install a bulky target which would extend to thicknesses in the sub-mm to mm regime. In the *prima facie* experiment at RAL a thick target consisting of MgO powder was used in which all protons were stopped [5]. This optimization of the target thickness was based on SRIM [26] calculations in which the condition was set that even the most energetic protons produced in the

experiment with $E_p \sim 9$ MeV are decelerated to energy values below the reaction threshold within the secondary target. A thickness of 1 mm was derived. SRIM can also be used to calculate the corresponding time t_{stop} by which all protons are reduced to kinetic energies below $E_p = 4.988$ MeV. It was found that within a duration of $t_{\text{stop}} = 100$ ps the electronic and nuclear stopping has reduced all impacting protons with $E_p \sim 9$ MeV to an energy below the reaction threshold in the chosen thick target. With respect to t_{stop} it is important to mention that the stopping of the fast protons occurs already during the time less energetic, hence slower, reaction-driving protons arrive at the target. Hence, a crude estimate of a maximal irradiation time of $t_{\text{irrad}} = 200$ ps ($\delta_{\text{TOF}} + t_{\text{stop}}$) can be assumed. Most importantly, for the case study on ^{26}Al , is the fact this value is still well below the lifetime of the crucial short-lived second excited state at 417 keV with $t_{1/2} = 1.20$ ns. With optimized geometry and targetry the assumed 200 ps value for t_{irrad} can easily be halved in future experiments with PW systems.

It is important to mention that HPLS will eventually be capable of producing macroscopic sheets of protons in which collective stopping effects will lead to a much-increased stopping power and hence reduced stopping times. In this work we do not consider these potential effects, but, as well as minimizing t_{irrad} , an enhanced stopping will result in higher plasma temperatures than those e.g., characterizing WDM conditions, offering new pathways for astrophysical investigations in the future.

3.2. Simulations of Population Yields for ^{26}Al obtained by a Short Pulsed Laser Proton Beam of High Intensity

Figure 2 shows the calculated distributions of $Y_{g.s.}$, Y_{228} and Y_{417} deduced from Equations (1) and (2) assuming $t_{\text{irrad}} = 200$ ps. The extracted values for the associated integral cross sections σ^{int} in the region between $E_p = 4.988$ MeV and $E_p = 5.820$ MeV were taken from Table 1. We assume the proton energy distribution, dN/dE_p , within this range to be constant as a first order approximation. The time zero $t_0 = 0$ which is truncated in the logarithmic display, refers to the time of the first reaction induced by the fastest protons arriving in the secondary production target. Although the yield depicted on the y -abscissa is in arbitrary units, a.u., the value is aligned with obtainable levels of concentration in units of 1 cm^{-3} deduced from the initial measurements of ^{26}mAl at the RAL. The values can be seen as a minimum estimate for achievable yield concentrations with a PW laser system. We assume all consecutive pulses to impact on the same volume within the secondary production target, hence the yield for $^{26}\text{Al}_{g.s.}$, $Y_{g.s.}$, builds up continuously after each pulse due to the very long lifetime of the ground state, $t_{1/2} = 0.717$ My. In addition, the ground state is populated by direct feeding from the 417 keV level (Equation (2)) which decays via an E2 transition (see Figure 1). As ^{26}Al is cosmogenic we can assume its original concentration in Mg or MgO , before the first shot, in the secondary target probe to be $Y_{g.s.}^0 \sim 0$. Moreover, we consider that two sequential proton pulses are separated by an interval of $t = 100$ s for simplicity which reflects roughly the time interval between two consecutive pulses from the 10 PW system at ELI-NP. As a result, the yield for ^{26}mAl , Y_{228} , does not build up between two consecutive shots which would be the case for the 1 PW and 0.1 PW systems at ELI-NP as they operate at higher repetition rates \sim Hz. Most interestingly is the fact that $\sigma_{g.s.}^{\text{int}}$ describing the direct population of the ground state, is significantly lower than for the excited states but builds up continuously in the active secondary target volume after each pulse due to its long lifetime. We calculated these conditions for a series of consecutive laser pulses, assuming the target to remain undamaged during the impact of all subsequent pulses. Crucially for the understanding of temporal yield evolution is the fact that the irradiation time $t < 200$ ps is still lower than the lifetime of the 417 keV state which allows this state to accrue comparable yields with regard to the first excited state at 228 keV per single pulse. For the first couple of pulses this is even true for a comparison with $Y_{g.s.}$ as can be derived from Figure 2. The two yields Y_{228} and Y_{417} remain unchanged for the two consecutive pulses shown in Figure 2 and for any additional subsequent pulse. This is a very special condition only achievable with the ultrashort pulses provided by an all-optical accelerator system. Consecutive pulses will only lead to higher values for $Y_{g.s.}$ in the same target volume.

For the near future, a total of several 100 pulses with a 10 PW laser system can be seen as a reasonable estimation for the number of total shots deliverable in a single experiment. With optimized target geometry, the appliance of proton focusing and PW induced proton pulses, potentially of mono-energetic nature, one can expect yields to be several orders of magnitude higher than those sketched in this work based on the RAL experiment. As shown in Table 1, the decay of the 511 keV delayed annihilation radiation will be the only measurable entity in any future laser-driven experiment while the other intensities would have to be calculated in reference to the precise cross-section data of Skelton et al. [18]. It is also important to point out that, if the irradiated volume is changed on a pulse-by-pulse base, each consecutive pulse will impact on a region where no measurable yield for $^{26}\text{Al}_{\text{g.s.}}$ existed before. The importance of that scenario and associated technical aspects will be depicted in the aforementioned forthcoming publication [6]. However, it is clear that due to the high costs of isotopically enriched ^{26}Mg an experiment relating on a constant supply of non-irradiated ^{26}Mg will be not feasible for budget and resourcing reasons.

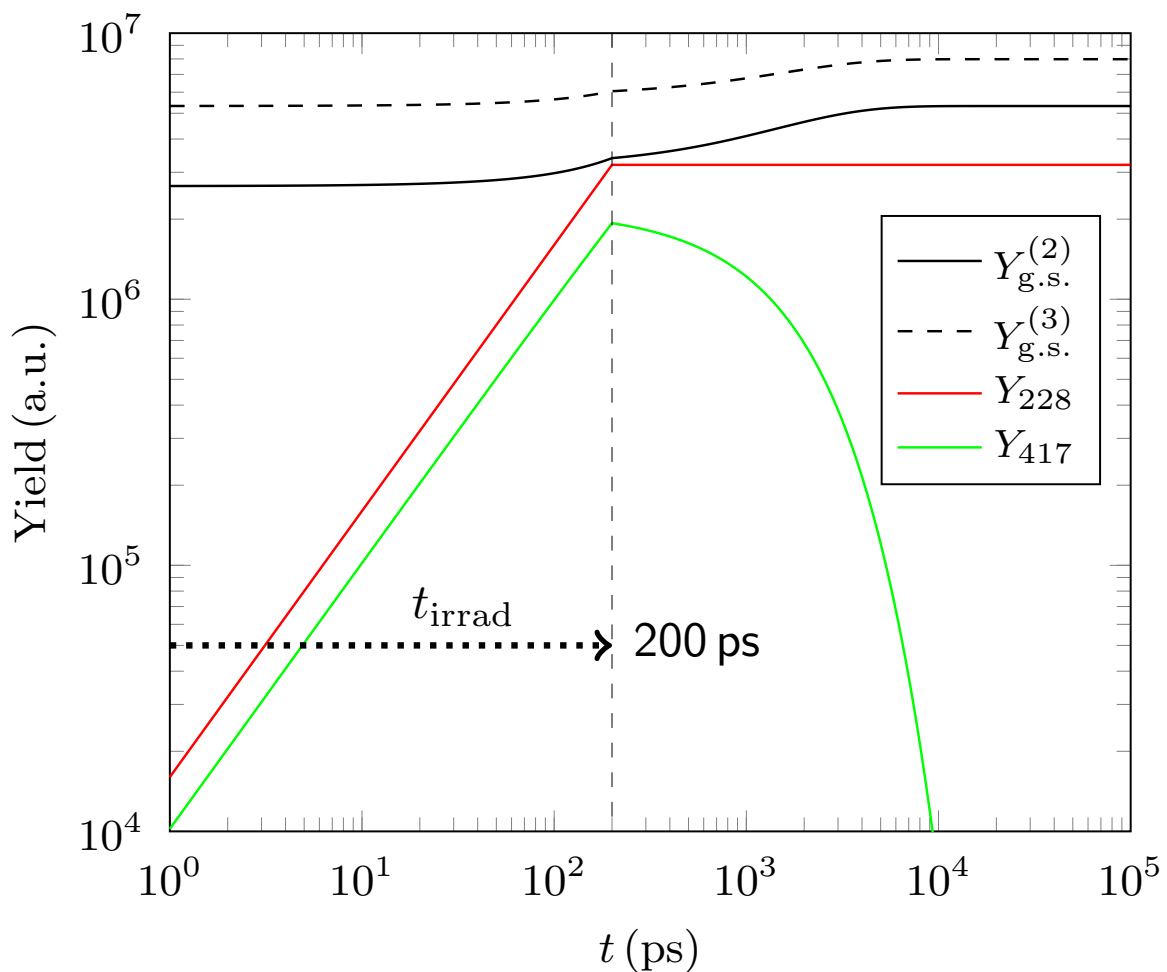


Figure 2. Calculated yields Y_{228} (red) and Y_{417} (green) as function of time t per proton pulse with $t_{\text{irrad}} = 200$ ps (vertical dashed line) and $4.988 \text{ MeV} \leq E_p \leq 5.820 \text{ MeV}$. The accumulated yields $Y_{\text{g.s.}}$ for the ground state are superimposed for the 2nd (solid black) and 3rd (dashed black) consecutive proton pulses. We assume those pulses to impact on the same target volume in the secondary production target. Note the influence of the direct feeding from the 417 keV level to the ground state from the non-linear enhancement of $Y_{\text{g.s.}}$ during t_{irrad} . A time interval of 100 s between the 2nd and 3rd pulse was assumed.

3.3. Thermodynamic Temperature Equivalents from the Distribution of the First Three Excited States in ^{26}Al in Laser Plasma Experiments

Using the Maxwell-Boltzmann distribution as depicted in Equation (4) the ratios of the two yield distributions; $Y_{228}/Y_{\text{g.s.}}$ and $Y_{417}/Y_{\text{g.s.}}$ were mapped into temperature equivalents to emphasize the unique ability of laser-driven experiments to facilitate the short, reaction-driving, ion pulses to mimic temperature-equivalent scenarios as present in hot interstellar conditions. In absence of a real hot plasma this interpretation exploits the fact that the hot state of the ^{26}Al compound residue is conserved for fleeting lifetimes after the reaction-driving pulse has impacted. The results for the consecutive pulses numbered, 1, 2, 3, 5, 10, 25, 50 and 100 are displayed in Figure 3.

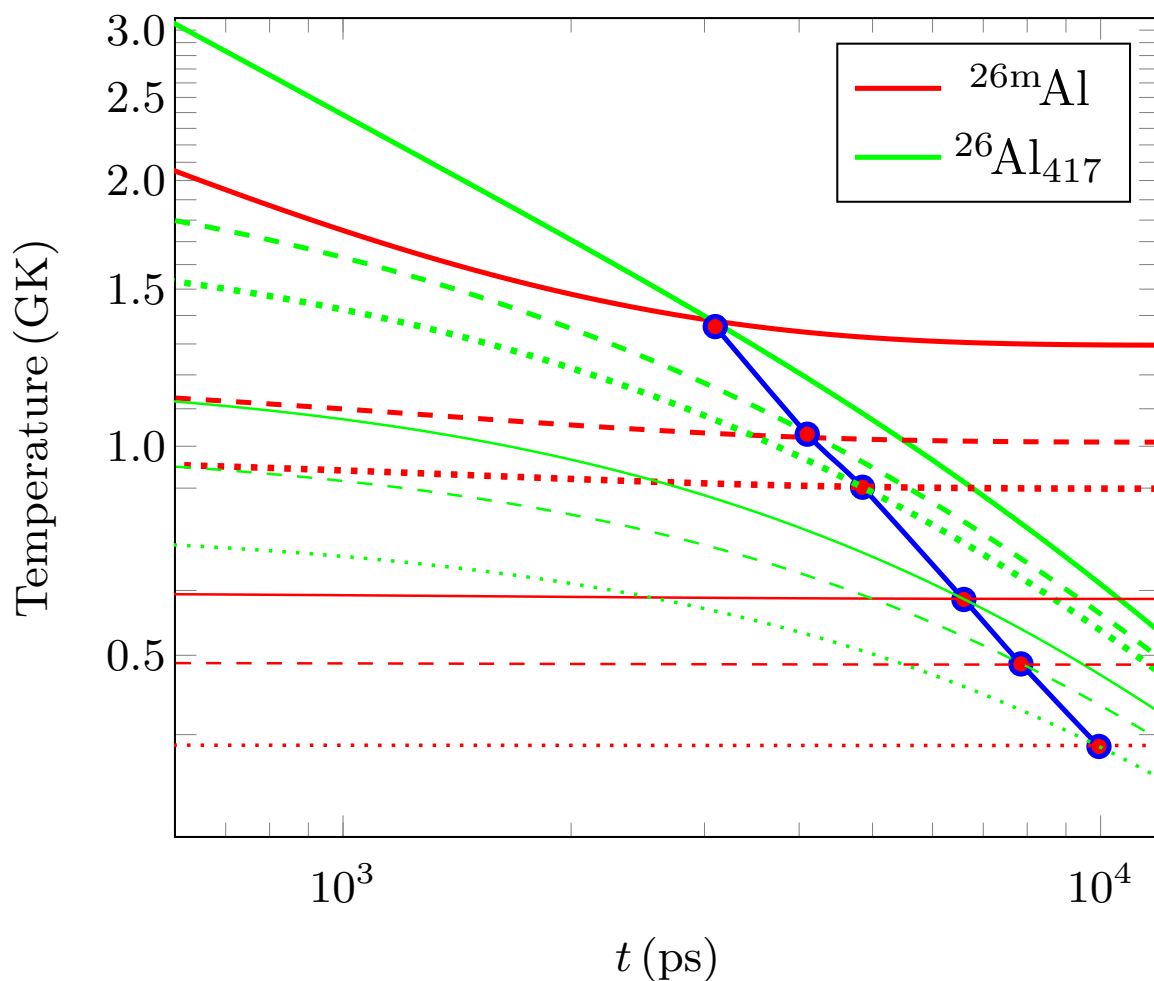


Figure 3. Calculated T equivalents for $Y_{228}/Y_{\text{g.s.}}$ (red lines) and $Y_{417}/Y_{\text{g.s.}}$ (green) from yield distributions according to Maxwell-Boltzmann distribution, for consecutive pulse numbers 1 (solid thick), 2 (dashed thick), 3 (dotted thick), 5 (solid thin), 25 (dashed thin) and 100 (dotted thin). The protons are considered to irradiate the same volume in the secondary target. The times t_{equi} for each pulse at which the two yield ratios converge to resemble one temperature value T are indicated by the blue & red circles which are connected to a blue line to guide the eye.

Theory states that to infer a temperature between the ground state and the first excited state in the case of ^{26}Al is not a straight forward concept, as those states are only connected via higher-lying excited states in low to middle temperature plasma. Nevertheless, the temperature equivalents between these two states, based on their yield population, remain in the GK temperature regime due to the short times of the populating laser proton pulse. At such high temperatures, thermalization can be assumed in stellar environments [21]. Most crucially, for any successive pulse there exist a defined

time t_{equi} , where the T equivalents of the first two excited states are equal, mimicking the conditions of a thermal equilibrium distribution in the absence of real hot temperature conditions in the production target. For the calculated cases, this regime stretches from 3.10 ns in which the temperature equivalent is 1.3 GK for the first pulse to 9.95 ns with $T = 0.4$ GK for the 100th pulse. Any probing X-ray flash or secondary ion beam would be best timed around t_{equi} to exploit that artificially stellar-like astrophysical scenario mimicking an equilibrium in hot plasma. It is worth noting that for consecutive runs, this particular time increases to almost 10 ns while the temperature-equivalent value decreases. The fact represents the natural buildup of the long-lived ground state.

Using RF-based technology the realization of such conditions characterized by yield distributions resembling high temperatures at short time intervals after reaction-triggering pulses is not possible. It is the shortness of the fastest transition that demands a short triggering high beam flux ϕ to achieve such scenarios. Moreover, the assumed high yields achievable with a HPLS system are multiple orders of magnitude higher than those of current RF-technology which summarizes the essence of the contribution these systems can provide for future astrophysical studies. Again, one needs to emphasize that we are not referring here to real hot plasma temperatures. It can be envisaged that, once mono-energetic laser proton pulses are achieved, the depicted calculation can be extended to include any of the 64 states below the proton separation energy $S_p = 6.306$ MeV threshold of ^{26}Al . Such a calculation will help in the understanding of the complex interplay between the short-lived states belonging to the e_1 and e_2 ensembles and the longer-lived low lying states as function of the temperature T thus allowing to study the evolution of the effective lifetime τ_{eff} for ^{26}Al .

3.4. Considerations about Measurability at HPLSs

The above work sketches the unique experimental reaction scenarios which can be established with the short pulses of high-power laser-driven system. Core to the considerations is the fact that short-lived states can be produced with high yields, which exhibit, in the depicted case of ^{26}Al a 1.9×10^{22} times shorter lifetime compared to that of the ground state. It is however important to consider the measurability of those scenarios in this work. First and foremost, in the case of ^{26}Al , the only measurable parameter at a high-power laser system will be, for the foreseeable future, the delayed 511 keV radiation. A measurement of the prompt radiation will stay elusive mainly to the EMP pulse which will not allow a direct deduction of the yield of the $t_{1/2} = 1.20$ ns at 417 keV. Current γ -ray detector systems placed at PW are maybe capable of resolving ms isomers at best [27]. Moreover, it is unlikely for any forthcoming HPLS system to host a sophisticated, efficient neutron detector system for inaugural experiments. To deduce yield changes in ^{26}Al independently of pulse-to-pulse variations, one could refer to a second reaction channel with a precisely measured cross-section that is triggered in coincidence with the production of ^{26}Al . The *prima facie* experiment therefore used MgO to compare changes in the yield ratio between ^{26m}Al and ^{13}N obtained via $^{16}\text{O}(p, \alpha)^{13}\text{N}$. Since the β^+ half-life of the resulting ^{13}N nucleus is 9.965 min the corresponding yield could be clearly distinguished from the super-allowed β^+ decay of ^{26m}Al with $t_{1/2} = 6.35$ s [6].

The beamlines at the ELI-NP facility are ideally suited to spearhead any related measurement. In Table 2 shows the core features of the ELI-NP HPLS characterized by their power P . The ELI-NP laser system has two equal arms allowing the synchronization of the two beams. The energy E_{pul} and pulse duration t_{pul} depicted for the laser pulse represent the average values as required from the THALES Group, the laser manufacturer in France. At the highest power of 10 PW a repetition rate f of 1 pulse per minute is foreseen. The intensity I_{pul} for the 10 PW is estimated to reach values in excess of 1×10^{23} Wcm $^{-2}$. At this intensity simulations provide a maximum proton energy E_p^{max} of a few 100 s of MeV, to be conservative. The corresponding values for the 0.1 PW and 1 PW systems are taken from published work [25]. Most importantly it can be seen that the least energetic 100 TW beamline can deliver protons above the reaction threshold, having additionally the advantage of a comparatively high repetition rate. It is however important to note that the mean beam currents achievable with any of the HPLS are still a few orders of magnitude smaller than those achievable with the conventional

RF-accelerator technology. The values supplied for I_p^{\max} describe the estimated ranges of the electrical peak currents induced by the reaction-driving protons from a single high-power laser pulse.

Table 2. Characteristic features of the high-power laser beamlines to be implemented at ELI-NP.

P/PW	E_{pul}/J	t_{pul}/fs	I_{pul}/Wcm^{-2}	f/Hz	E_p^{\max}/MeV	I_p^{\max}
10	250	25	10^{22-23}	0.017	>200	kA-MA
1	25	25	10^{21-22}	1	~100	A-kA
0.1	2.5	25	10^{20-21}	10	~30	mA-A

Our presented paper should be seen as a guideline for development, pointing out the possibilities, rather than an experimental proposal form. It is however hoped that with ever increasing fluxes ϕ , optimized geometry and high laser-to-proton energy conversion obtainable by the next generation of multi-PW laser plasma accelerators the total obtainable yields for the production of ^{26}Al will provide densities in the order of $1 \times 10^{10} \text{ cm}^{-3}$ and possibly even much higher. With improved values for laser energy-to- γ -conversion, a second laser beam in coincidence could therefore be used to probe the coupling of excited states by photo-excitation transitions by supplying a secondary, intense, X-ray beam. This will allow, potentially, the characterization of a yield change of Y_{228} in the presence of a hot photon bath. An enhancement of Y_{228} in such a case would be a first indication of the onset of an equilibrium between the ground and first excited state via the coupling of the e_1 and e_2 ensembles in ^{26}Al [21]. Moreover, such a study could enable to understand the intricate interplay between the excited states which govern the λ_{eff} . As current theories only account for a fraction of the abundance of ^{26}Al one may expect that a more elaborate evaluation of the effective lifetime will better reflect the production and decay mechanisms in actual astrophysical scenarios explaining the measured surplus of ^{26}Al in our Galaxy.

From the depicted scenarios, it is clear that an online isotope separator facility which uses a Penning-trap would be an ideal extension to improve any related experiment as it would allow a direct identification of $^{26}\text{Al}_{\text{g.s.}}$ as well as supporting the measurement of $^{26\text{m}}\text{Al}$. It is hoped to implement such a system eventually at the experimental stations dedicated to nuclear reaction research at ELI-NP.

4. Conclusions

We presented a pathway for high-power laser physics at the interface of nuclear astrophysics. The example of ^{26}Al showed that laser systems can provide short-lived states in high yields, comparable with those states that exhibit much longer lifetimes. This feature is unique to HPLS due to the ability of all-optical accelerator systems to deliver high temporal fluxes ϕ of reaction-driving protons for the fleeting time spans in the order of the lifetimes of the shortest-lived excited states. Exploiting the fact that the high temperatures within the residual ^{26}Al nuclei prevail for some ultrashort duration after its creation by a compound reaction, high entropy conditions in cold plasma environments can be achieved and potentially be tested with a second radiation or particle beam. In the case of ^{26}Al the yield ratios, $Y_{228}/Y_{\text{g.s.}}$ and $Y_{417}/Y_{\text{g.s.}}$, interpreted in the framework of the Maxwell-Boltzmann statistics, were found to mimic thermal equilibrium at defined times t_{equi} in the range of 300 ps to 10 ns resembling thermalization in a fictitious GK plasma environment. This circumstance can help in future experiments in the quest to create a nuclear astrophysical laboratory. In this respect, future investigations could be the application of coinciding X-ray pulses of high intensities, or an additional proton beam creating WDM. The study of other isotopes and the interplay of their excited states maybe envisaged with, e.g., ^{34}Cl , ^{115}In and ^{180}Ta being other very interesting cases for future investigation [20,21].

Author Contributions: K.M.S. conceived and designed the idea and theoretical planning; D.D. suggested and scrutinized the laser systems abilities regarding the paper; B.S.M. supported and revised the theoretical aspects regarding the entropy conditions as stated.

Funding: This research received no external funding.

Conflicts of Interest: The authors declare no conflict of interest.

Abbreviations

The following abbreviations are used in this manuscript:

CPA	Chirped pulse amplification
ELI-NP	Extreme Light Infrastructure-Nuclear Physics
EMP	Electromagnetic pulse
GCNDS	Graphite-cube neutron-detection system
HPLS	High-power laser system
RAL	Rutherford Appleton Laboratory
TNSA	Target normal sheath acceleration
TOF	Time-of-flight
WDM	Warm dense matter

References

- Hauser, W.; Feshbach, H. The Inelastic Scattering of Neutrons. *Phys. Rev.* **1952**, *87*, 366–373. [[CrossRef](#)]
- Strickland, D.; Mourou, G. Compression of amplified chirped optical pulses. *Opt. Commun.* **1985**, *56*, 219–221. [[CrossRef](#)]
- Bateman, H. The solution of a system of differential equations occurring in the theory of radioactive transformations. *Proc. Camb. Philos. Soc.* **1910**, *15*, 423–427.
- Morrissey, D.J.; Bloch, C.; Benenson, W.; Kashy, E.; Blue, R.A.; Ronningen, R.M.; Aryaeinejad, R. Thermal population of nuclear excited states. *Phys. Rev. C* **1986**, *34*, 761–763. [[CrossRef](#)]
- Denis-Petit, D.; Ledingham, K.W.D.; McKenna, P.; Mascali, D.; Tudisco, S.; Spohr, K.M.; Tarisien, M. Nuclear Reactions in a Laser-Driven Plasma Environment. In *Applications of Laser-Driven Particle Acceleration*; Bolton, P., Parodi, K., Schreiber, J., Eds.; CRC-Press, Taylor & Francis Group: Boca Raton, FL, USA, 2018; Chapter 22, pp. 339–352.
- Spohr, K.M.; Ledingham, K.W.D.; Clarke, R.; Carroll, D.C.; Doria, D.; Gray, R.J.; Hassan, M.; Labiche, M.; McCanny, T.; McKenna, P.; et al. Unpublished work, 2019.
- Patel, P.K.; Mackinnon, A.J.; Key, M.H.; Cowan, T.E.; Foord, M.E.; Allen, M.; Price, D.F.; Ruhl, H.; Springer, P.T.; Stephens, R. Isochoric Heating of Solid-Density Matter with an Ultrafast Proton Beam. *Phys. Rev. Lett.* **2003**, *91*, 125004. [[CrossRef](#)] [[PubMed](#)]
- Ping, Y.; Correa, A.; Ogitsu, T.; Draeger, E.; Schwegler, E.; Ao, T.; Widmann, K.; Price, D.; Lee, E.; Tam, H.; et al. Warm dense matter created by isochoric laser heating. *High Energy Density Phys.* **2010**, *6*, 246–257. [[CrossRef](#)]
- Thirolf, P.G.; Habs, D.; Gross, M.; Allinger, K.; Bin, J.; Henig, A.; Kiefer, D.; Ma, W.; Schreiber, J. Fission-Fusion: A new reaction mechanism for nuclear astrophysics based on laser-ion acceleration. *AIP Conf. Proc.* **2011**, *1377*, 88–95.
- Oginni, B.; Iliadis, C.; Champagne, A. Theoretical evaluation of the reaction rates for $^{26}\text{Al}(n,p)^{26}\text{Mg}$ and $^{26}\text{Al}(n,\alpha)^{23}\text{Na}$. *Phys. Rev. C* **2011**, *83*, 025802. [[CrossRef](#)]
- Mahoney, W.A.; Ling, J.C.; Wheaton, W.A.; Jacobson, A.S. HEAO₃ discovery of ^{26}Al in the interstellar medium. *Astrophys. J.* **1984**, *286*, 578–585. [[CrossRef](#)]
- Arnould, M.; Norgaard, H.; Thielemann, F.K.; Hillebrandt, W. Synthesis of ^{26}Al in explosive hydrogen burning. *Astrophys. J.* **1980**, *237*, 931–950. [[CrossRef](#)]
- Arnett, W.D. Explosive Nucleosynthesis in Stars. *Astrophys. J.* **1969**, *157*, 1369. [[CrossRef](#)]
- Diehl, R.; Halloin, H.; Kretschmer, K.; Lichti, G.; Schönfelder, V.; Strong, A.; von Kienlin, A.; Wang, W.; Jean, P.; Knödseder, J.; et al. Radioactive ^{26}Al from massive stars in the Galaxy. *Nature* **2006**, *439*, 45–47. [[CrossRef](#)] [[PubMed](#)]
- Lee, T.; Papanastassiou, D.; Wasserburg, G. Demonstration of ^{26}Mg excess in Allende and evidence for ^{26}Al . *Geophys. Res. Lett.* **1976**, *3*, 41–44. [[CrossRef](#)]
- Villeneuve, J.; Chaussidon, M.; Libourel, G. Homogeneous Distribution of ^{26}Al in the Solar System from the Mg Isotopic Composition of Chondrules. *Science* **2009**, *325*, 985–988. [[CrossRef](#)] [[PubMed](#)]

17. Kita, N.T.; Yin, Q.Z.; MacPherson, G.J.; Ushikubo, T.; Jacobsen, B.; Nagashima, K.; Kurahashi, E.; Krot, A.N.; Jacobsen, S.B. ^{26}Al - ^{26}Mg isotope systematics of the first solids in the early solar system. *Meteorit. Planet. Sci.* **2013**, *48*, 1383–1400. [[CrossRef](#)]
18. Skelton, R.; Kavanagh, R.; Sargood, D. $^{26}\text{Mg}(p, n)^{26}\text{Al}$ and $^{23}\text{Na}(\alpha, n)^{26}\text{Al}$ Reactions. *Phys. Rev. C* **1987**, *35*, 45–54. [[CrossRef](#)]
19. Ward, R.A.; Fowler, W.A. Thermalization of long-lived nuclear isomeric states under stellar conditions. *Astrophys. J.* **1980**, *238*, 266–286. [[CrossRef](#)]
20. Coc, A.; Porquet, M.G.; Nowacki, F. Lifetimes of ^{26}Al and ^{34}Cl in an astrophysical plasma. *Phys. Rev. C* **1999**, *61*, 015801. [[CrossRef](#)]
21. Gupta, S.; Meyer, B. Internal equilibration of a nucleus with metastable states: ^{26}Al as an example. *Phys. Rev. C* **2001**, *64*, 025805. [[CrossRef](#)]
22. Dunford, C.; Burrows, T. *Online Nuclear Data Service*; Report IAEA-NDS-150; NNDC Informal Report NNDC/ONL-95/10; BNL National Nuclear Data Center: Brookhaven, NY, USA, 1996; p. 015801.
23. Äystö, J.; Eronen, T.; Jokinen, A.; Kankainen, A.; Moore, I.; Penttilä, H. An IGISOL portrait. *Hyperfine Interact.* **2013**, *223*, 1–3. [[CrossRef](#)]
24. Wilks, S.C.; Langdon, A.B.; Cowan, T.E.; Roth, M.; Singh, M.; Hatchett, S.; Key, M.H.; Pennington, D.; MacKinnon, A.; Snavely, R.A. Energetic proton generation in ultra-intense laser–solid interactions. *Phys. Plasmas* **2001**, *8*, 542–549. [[CrossRef](#)]
25. Higginson, A.; Gray, R.J.; King, M.; Dance, R.J.; Williamson, S.D.R.; Butler, N.M.H.; Wilson, R.; Capdessus, R.; Armstrong, C.; Green, J.S.; et al. Near-100 MeV protons via a laser-driven transparency-enhanced hybrid acceleration scheme. *Nat. Commun.* **2018**, *9*, 724. [[CrossRef](#)] [[PubMed](#)]
26. Ziegler, J.F.; Ziegler, M.D.; Biersack, J.P. SRIM—The stopping and range of ions in matter. *Nucl. Instrum. Methods Phys. Res. B* **2010**, *268*, 1818–1823. [[CrossRef](#)]
27. Negoita, F.; Roth, M.; Thierolf, P.G.; Tudisco, S.; Hannachi, F.; Moustazis, S.; Pomerantz, I.; McKenna, P.; Fuchs, J.; Spohr, K.M.; et al. Laser Driven Nuclear Physics at ELI-NP. *Rom. Rep. Phys.* **2016**, *68*, S37–S144.



© 2018 by the authors. Licensee MDPI, Basel, Switzerland. This article is an open access article distributed under the terms and conditions of the Creative Commons Attribution (CC BY) license (<http://creativecommons.org/licenses/by/4.0/>).